Climate-Driven Weathering Shifts Between Highlands and Floodplains

Zhaojie Yu, Christophe Colin, Franck Bassinot, Shiming Wan, Germain Bayon

Geochemistry, Geophysics, Geosystems

RESEARCH ARTICLE
10.1029/2020GC008936

Key Points:
- Orbital-millennial clay records in Northern Indian Ocean of past 190 and 80 kyr are reported
- Climate change results in a shift from mountain- to floodplain-dominated weathering regimes
- Possible impact of climate-driven weathering regimes in mountainous watersheds on carbon cycle

Supporting Information:
- Table S1

Correspondence to:
Z. Yu,
yuzhaojie@qdio.ac.cn

Citation:
Yu, Z., Colin, C., Bassinot, F., Wan, S., & Bayon, G. (2020). Climate-driven weathering shifts between highlands and floodplains. *Geochemistry, Geophysics, Geosystems*, *21*, e2020GC008936. https://doi.org/10.1029/2020GC008936

Received 22 JAN 2020
Accepted 4 JUN 2020
Accepted article online 9 JUN 2020

Climate-Driven Weathering Shifts Between Highlands and Floodplains

Zhaojie Yu[1,2,3], Christophe Colin[4], Franck Bassinot[5], Shiming Wan[1,2,3], and Germain Bayon[6]

[1]Key Laboratory of Marine Geology and Environment, Institute of Oceanology, Chinese Academy of Sciences, Qingdao, China, [2]Laboratory for Marine Geology, Qingdao National Laboratory for Marine Science and Technology, Qingdao, China, [3]Center for Ocean Mega-Science, Chinese Academy of Sciences, Qingdao, China, [4]Laboratoire GEOsciences Paris-Sud (GEOPS), UMR 8148, CNRS-Université de Paris-Sud, Université Paris-Saclay, Orsay Cedex, France, [5]Laboratoire des Sciences du Climat et de l'Environnement, LSCE/IPSL, CEA-CNRS-UVSQ, Université Paris-Saclay, Gif-sur-Yvette, France, [6]Marine Geosciences Unit, IFREMER, Plouzané, France

Abstract Chemical weathering of silicate rocks on continents is thought to have played an important role in the evolution of past atmospheric carbon dioxide over geologic timescales. However, the detailed links between continental weathering and climate change over shorter timescales, and their potential impact on sediment records deposited in the ocean, remain poorly understood. Here, we present clay mineralogy and strontium-neodymium isotopic data for marine sediment records from the Northern Indian Ocean, with the aim of investigating the weathering response of large Himalayan river basins to orbital and millennial climate forcing. We show that past glaciated episodes of the late Quaternary corresponded to periods of increased physical erosion, associated with the preferential export of illite and chlorite assemblages from the Himalayan highlands having relatively radiogenic Sr isotopic signatures. In contrast, the warm periods of enhanced monsoon rainfall coincided with the transport of intensively weathered smectite-dominated soils derived from the floodplains, characterized by lower $^{87}Sr/^{86}Sr$ signatures. This finding suggests that the short-term climatic variability over late Quaternary timescales was accompanied by concomitant changes between high mountain- versus floodplain-dominated weathering regimes, with possible impact on the nature of weathered rocks and, as a consequence, on the carbon cycle.

1. Introduction

Continental weathering of silicate rocks has long been proposed as an important regulator of Earth's climate over geologic timescales, through consumption of atmospheric CO_2 and subsequent carbonate precipitation in the ocean (Garrels et al., 1976; Raymo & Ruddiman, 1992; West et al., 2005). This conventional view has been challenged by field observations suggesting that weathering in high mountain and glaciated environments could act instead as a source of atmospheric CO_2 via oxidation of fossil organic matter and sulfide minerals (Horan et al., 2017; Torres et al., 2014, 2016). In parallel, recent studies have shown that continental weathering could react rapidly to short-term climate changes and other environmental disturbances, as inferred from recent modeling (Beaulieu et al., 2012) and various field observations based on geochemical proxies (Bastian et al., 2017; Dosseto et al., 2015; Miriyala et al., 2017). Nevertheless, the climatic control of chemical weathering over recent geological timescales, such as during the late Quaternary for instance, and its environmental impacts, still remain unclear (Gaillardet et al., 1999; Millot et al., 2002; West, 2012). Clearly, understanding the links between abrupt climate change and the rate and intensity of continental weathering on continents, especially the complex relationship between physical erosion, chemical weathering, climate, and sediment source-to-sink processes, requires further investigations (Burbank et al., 2003; Dosseto et al., 2015; Tipper et al., 2006; Vance et al., 2009). In particular, the prediction accuracy of future levels of greenhouse gases in the atmosphere calls for a better understanding of the potential factors influencing the evolution of past atmospheric CO_2 and their response to climate change.

South Asia displays the highest density of glaciers outside polar regions and is strongly influenced by Indian Summer Monsoon (ISM) precipitation. As such, it represents a key region to investigate the interplay between climate, mountain erosion, and continental weathering through time. Regional paleoclimate studies indicate synchronous variations of ISM not only with low latitude solar radiation in the northern

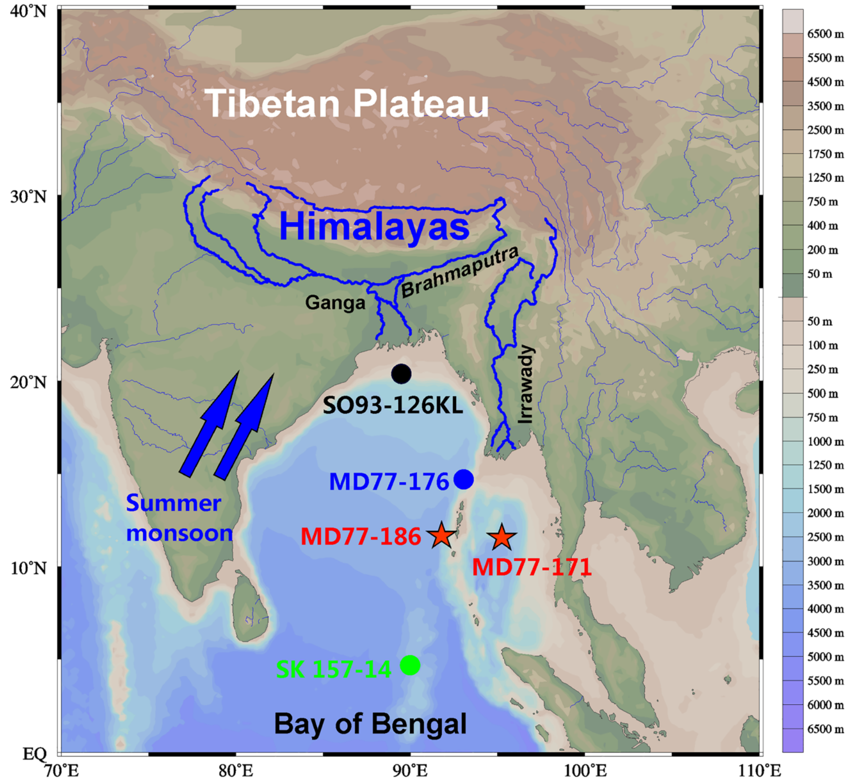

Figure 1. Bathymetric map showing the location of cores MD77-186 in the Bay of Bengal (BoB) and MD77-171 in the Andaman Sea (red stars) as well as the reference sites in the BoB: cores SO93-126KL, MD77-176, and SK157-14. Nearby Himalayan river systems: Ganges-Brahmaputra (G-B) River and the Irrawaddy River are also shown. Indian Summer Monsoon (ISM) is marked as blue arrows.

hemisphere (Clemens et al., 1991; Kathayat et al., 2016) but also with millennial-scale North Atlantic climatic oscillations through atmospheric and oceanic teleconnections (Deplazes et al., 2014; Kudrass et al., 2001; Tierney et al., 2015). While it has already been suggested that past changes in monsoon precipitation and temperature had influenced both weathering rate and intensity during the late Quaternary, as well as the export of riverine sediment loads from South Asia river catchments (Alizai et al., 2012; Burton & Vance, 2000; Colin et al., 1999; Goodbred & Kuehl, 2000; Hu et al., 2013; Lupker et al., 2013; Miriyala et al., 2017; Stoll et al., 2007), the response and of chemical weathering patterns over short-term climatic forcing, and its potential impact of carbon cycling, has not been investigated so far.

Here, we performed ^{14}C AMS and δ^{18}O stratigraphy, clay mineralogy, and geochemical measurements of two marine sediment cores: MD77-186 (11°27′5N, 92°00′0E, water depth 890 m) and MD77-171 (11°45′6N, 94°09′0E, water depth 1,760 m), located in the Bay of Bengal (BoB) and the Andaman Sea, respectively, to investigate the impact of orbital-millennial climate changes on erosion and weathering in Himalayan river basins during the late Quaternary. Colin et al. (1999) have already reported various clay mineralogical and major element data for two sediment cores in this area, aimed at establishing the impact of climate changes on the weathering and erosion of the Himalayan and Burman ranges during glacial–interglacial cycles. In this study, we present new proxy records from cores MD77-186 and MD77-171 that reveal the response of high mountain- versus floodplain-dominated weathering regimes to orbital-millennial climate changes and its potential impact on global carbon cycling.

2. Methods

2.1. Sediment Cores and Age Model

Cores MD77-186 and MD77-171 were collected in the northern Indian Ocean by the R/V *Marion Dufresne* (Figure 1). The lithology of both cores consists of brown nannofossil ooze with interbedded silty clay and

Table 1
Accelerator Mass Spectrometry (AMS) ^{14}C Dates of Monospecific Planktonic Foraminifera From Core MD77-186

Depth (cm)	^{14}C age (year)	Error (year)
45–50	6,214	30
101–106	7,371	30
170–175	13,591	30
215–220	15,892	50
270–275	21,227	60
330–335	25,894	90
400–405	40,322	140
440–445	42,316	690

silty sand. The age model for core MD77-186 is based on eight accelerator mass spectrometry (AMS) ^{14}C dates of monospecific planktonic foraminifera (Table 1) and the tuning of planktonic foraminifera Globigerinoides ruber $\delta^{18}O$ (Table S1 in the supporting information) to the LR04 record (Lisiecki & Raymo, 2005). For the last 40 kyr of core MD77-186, the Calib 4.1 program was used to convert the ^{14}C ages into calendar ages (Stuiver et al., 1998), which includes a 400-year correction for the ocean surface reservoir age (Broecker & Peng, 1982). The age model for radiocarbon dates older than ^{14}C BP > 40 kyr was established using the $\delta^{18}O$ correlation to the LR04 stack record.

The planktonic foraminifera G. ruber $\delta^{18}O$ downcore trend of MD77-171 is tuned to the LR04 record using Analyseries software to establish an age model. For cores MD77-186 and MD77-171, G. ruber $\delta^{18}O$, expressed in ‰ versus Vienna Pee Dee Belemnite standard (VPDB), were obtained from analyses of about 10 foraminifera shells from 250 to 315 μm size range. Analyses were performed on a MAT251 mass spectrometer at the Laboratoire des Sciences du Climat et de l'Environnement (LSCE), France. Data are reported versus PDB after calibration with NBS19. The mean external reproducibility of carbonate standards is ±0.05‰ for $\delta^{18}O$.

Based on those chronological frameworks, the volcanic ash layers observed at 596 to 600 cm in core MD77-186 and 770 to 774 cm in core MD77-171 appear to correspond to the Youngest Toba Tuff (YTT), with a calibrated $^{40}Ar/^{39}Ar$ age of 73.88 ± 0.32 kyr (Storey et al., 2012), thus providing an additional age control point (Figure 2). Consequently, the 6.2-m-long sediment record of core MD77-186 provides a continuous record of the period between 79.3 and 6.5 kyr, with an average linear sedimentation rate (LSR) of 7.8 cm/kyr (ranging from 5.8 to 10.2 cm/kyr), while the 14.2-m-long record of core MD77-171 covers the last 188.6 to 0.4 kyr, with an average LSR of 7.5 cm/kyr (ranging from 5.3 to 12.1 cm/kyr) (Figure 2). Cores MD77-186 and MD77-171 provide continuous records of the detrital sediment exported from large Himalayan river systems over the past 80 and 190 kyr, respectively.

2.2. Clay Mineral XRD

Clay mineralogical analyses were processed on a total of 243 samples for core MD77-186 (~0.3 kyr/sample) and 130 samples for MD77-171 (~1.5 kyr/sample). Sediments were first treated in order to remove carbonate material and organic matter using acetic acid (25%) and hydrogen peroxide (15%), respectively. Then, the clay mineral composition was determined on detrital sediment particles smaller than 2 μm, after separation based on the Stoke's settling velocity principle. The X-ray diffraction (XRD) analysis of clay mineral assemblages was carried on a PANalytical diffractometer at Laboratoire GEOsciences Paris-Sud (GEOPS), Université Paris-Saclay. For each sample, three XRD measurements were conducted: (1) after drying at room temperature, (2) after ethylene-glycol solvation for 24 hr, and (3) after heating at 490°C for 2 hr. The position of the (001) series of basal reflections on the above three XRD diagrams were used to identify the different clay minerals. The MacDiff software was used on the glycolated curve to semiquantitatively estimate the peak areas of the basal reflections for the main clay mineral groups (smectite 15–17 Å, illite 10 Å, and kaolinite/chlorite 7 Å). The ratio from the 3.57/3.54 Å peak areas was used to obtain the relative proportions of kaolinite and chlorite. The accuracy of one test sample analyzed during the course of this study was ±2% (2σ). Based on the XRD method, the semiquantitative weight content of each mineral phase was systematically better than 4%.

Additionally, illite chemistry index was calculated using the ratio of the peak areas for 5 and 10 Å illite in the ethylene-glycolated samples (Colin et al., 1999). The samples associated with ratios <0.4 represent Fe-Mg-rich illites (e.g., biotites and micas) that are likely to be indicative of physical erosion, while strong chemical hydrolysis are generally producing Al-rich illites, with a chemistry index >0.4 (Petschick et al., 1996).

2.3. Sr-Nd Isotopes and Grain Size

The Sr-Nd isotopic compositions and grain size were analyzed on 11 detrital sediment samples of core MD77-186. Sample preparations and analyses have been carried out following the analytical procedure described in detail by Yu et al. (2019). Briefly, the detrital fraction of the sediment was isolated after a

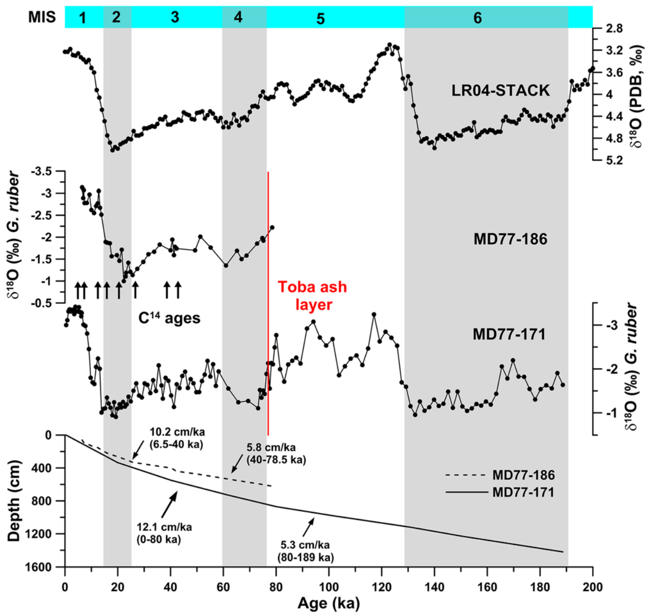

Figure 2. Age models for cores MD77-186 and MD77-171 in this study. The age model of core MD77-186 is based on accelerator mass spectrometry (AMS) ^{14}C dates (8 monospecific planktonic foraminifera dates) and oxygen isotope measurements (correlating the planktonic foraminifera *Globigerinoides ruber* $\delta^{18}O$ of core MD77-186 and the LR04 record). The planktonic foraminifera *Globigerinoides ruber* $\delta^{18}O$ downcore trend of MD77-171 is tuned to the LR04 record using Analyseries software to establish an age model. Note that the Youngest Toba Tuff (YTT) with a calibrated $^{40}Ar/^{39}Ar$ age of 73.88 ± 0.32 kyr is marked by red line.

sequential leaching procedure based on the use of acetic acid (25%) and hydrogen peroxide (15%), following the same procedure as described above. Then, samples were prepared at the Laboratoire GEOsciences Paris-Sud (GEOPS), Université Paris-Saclay for grain size analysis on a Malvern Mastersizer 2000 HYDROG. The reproducibility of grain size measurement is generally better than 2%.

The remaining detrital fraction was digested using concentrated HF, prior to separation of Sr and Nd fractions by ion chromatography. The Sr and Nd isotopic compositions were determined at the Laboratoire des Sciences du Climat et de l'Environnement (LSCE), Gif-sur-Yvette, France, using a Thermo Scientific Multi-Collector Induced Coupled Plasma Mass Spectrometer (MC-ICP-MS NEPTUNE^{Plus}). All samples (including standard solutions) were diluted to 20 ppb for analysis. The Sr NIST SRM987 ($^{86}Sr/^{88}Sr \approx 0.710250$) and Nd La Jolla ($^{146}Nd/^{144}Nd \approx 0.511858 \pm 0.000007$) (Lugmair et al., 1983) standard solutions were analyzed every two samples during corresponding analytical sessions. The mass fractionation biases on measured Sr and Nd isotopic ratios were corrected after normalization to $^{146}Nd/^{144}Nd = 0.7219$ and $^{86}Sr/^{88}Sr = 0.1194$, respectively, using an exponential law. Nd results are expressed as $\varepsilon_{Nd}(0) = [((^{143}Nd/^{144}Nd_{meas})/0.512638) - 1] \times 10{,}000$, using the CHUR value given by Jacobsen and Wasserburg (1980). The analytical error for each sample analysis was taken as the external reproducibility of the La Jolla standard unless the internal error was larger.

3. Results

3.1. Clay Mineralogy

The clay mineral assemblage of core MD77-186 is dominated by smectite (68–98%, average 88%), followed by illite (1–18%, average 6%), chlorite (1–8%, average 3%), and kaolinite (1–7%, average 3%) (Figure 3 and Table S2). Similarly, the majority clays for core MD77-171 also corresponds to smectite (55–87%, average 70%), with minor contributions from illite (5–22%, average 13%), chlorite (5–13%, average 9%), and kaolinite (2–13%, average 9%) (Figure 3 and Table S3). The illite chemical index in core MD77-186 presents a range of variation between 0.2 and 0.5 with an average of 0.3, while varying from 0.3 to 0.5 (average of 0.4) for MD77-171 (Figure 3). The crystallinity of illite varies between 0.10 and 0.37° $\Delta 2\theta$ with an average value of 0.16° $\Delta 2\theta$ for MD77-186, while it ranges from 0.10° to 0.30° $\Delta 2\theta$ with an average value of 0.20° $\Delta 2\theta$ for MD77-171 (Figure 3).

As the variations of smectite in cores MD77-186 and MD77-171 are inversely related to illite, chlorite, and kaolinite contents, the smectite/(illite + chlorite) ratio appears well suited to characterize any mineralogical changes in the studied clay-size fractions (Figure 3). Smectite/(illite + chlorite) ratios in cores MD77-186 and MD77-171 range from 3.2 to 53.9 (average of 14.8) and from 0.9 to 12.2 (average of 3.4), respectively.

3.2. Sr-Nd Isotopes

The Sr ($^{87}Sr/^{86}Sr$) and Nd (ε_{Nd}) isotopic compositions of the 11 detrital fractions investigated in this study are listed Table 2. These samples cover the period that extends from the Last Glacial Maximum (LGM), deglaciation, and the Holocene, showing a range of $^{87}Sr/^{86}Sr$ ratios, from 0.7146 to 0.7246, while ε_{Nd} values oscillate between −11.4 and −9.2.

4. Discussion

4.1. Sediment Provenance and Strontium Isotope Decoupling During Weathering

The provenance of detrital sediment sources in marine sediments can be traced using ε_{Nd} and $^{87}Sr/^{86}Sr$, although $^{87}Sr/^{86}Sr$ changes in sediment records can also partly relate to their degree of chemical weathering and grain size (Goldstein & Hemming, 2003). No significant correlations between the mean grain size versus

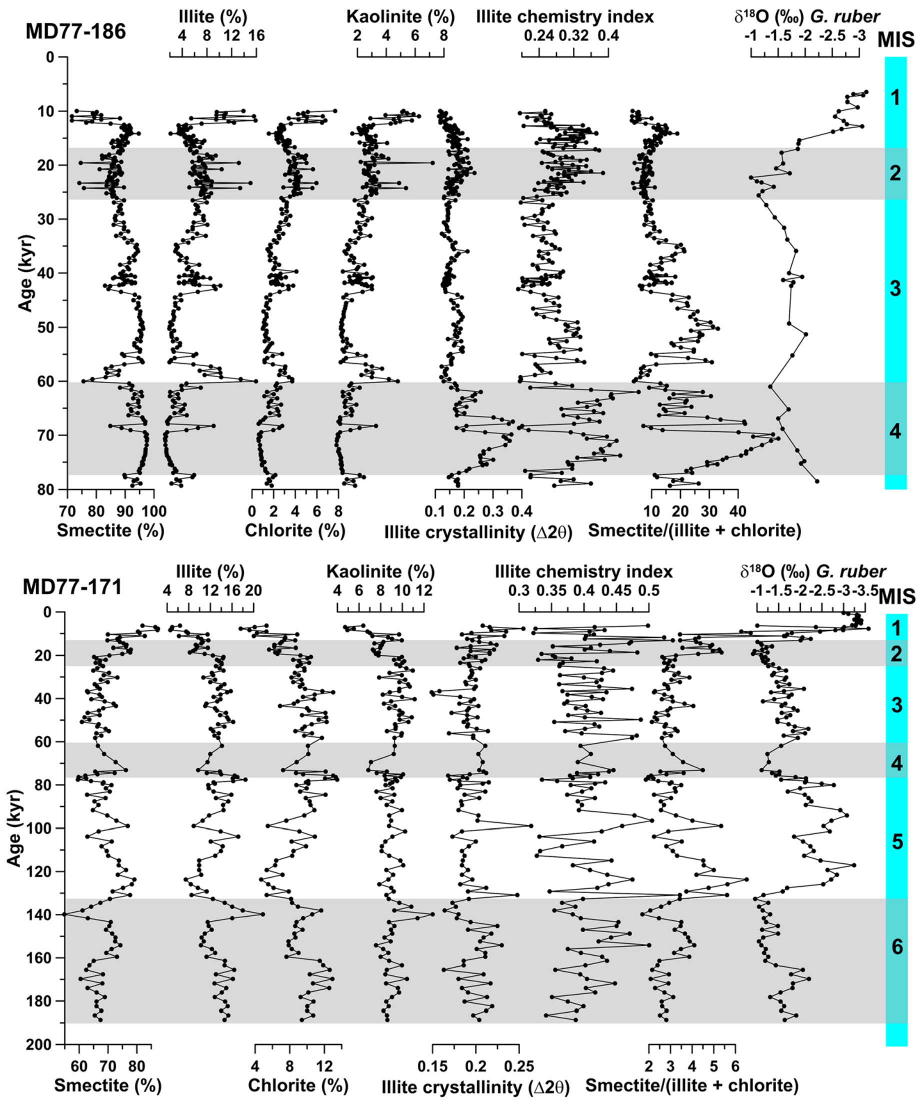

Figure 3. Clay mineral assemblages of core MD77-186 and MD77-171.

ε_{Nd} ($R^2 = 0.01$, $p < 0.01$, Figure 4a) and $^{87}Sr/^{86}Sr$ ($R^2 = 0.001$, $p < 0.01$, Figure 4b) from MD77-186 were observed in this study, implying that any significant grain size effect on Sr and Nd isotopes related to weathering and sediment transport is probably insignificant at the studied site.

Since the late Quaternary, the sediments delivered to the BoB have been mostly derived from the Ganges-Brahmaputra (G-B) river system, with reduced inputs from the Indo-Burman Ranges and the Irrawaddy River in the northeast bay, and minor contributions from Indian Peninsula rivers in the western bay (Colin et al., 1999; Joussain et al., 2016; Liu et al., 2019; Lupker et al., 2013). In this study, Sr and Nd isotopes are in agreement with core MD77-186 sediments being derived from a mixture between the G-B River, Indo-Burman Ranges, and the Irrawaddy River sources (Figure 4c). The G-B River ($^{87}Sr/^{86}Sr$ from 0.720 to 0.780 and ε_{Nd} from −18 to −14), which mainly brings sediments from the physically denuded high Himalayas and chemically weathered floodplain, has been considered as the most important sediment sources to marine sediments deposited in the BoB (Lupker et al., 2013; Singh & France-Lanord, 2002). Besides, many small rivers, such as the Koum and Karnaphuli Rivers, which drain the Indo-Burman Ranges, also supply sediments to the eastern BoB (Colin et al., 1999; Joussain et al., 2016). The Indo-Burman Ranges are composed of Neogene and Paleogene sedimentary rocks, ophiolites, serpentinites, and metamorphic rocks of Triassic to Cretaceous age, yielding sediment yields characterized by low $^{87}Sr/^{86}Sr$

Table 2
$^{87}Sr/^{86}Sr$, $^{143}Nd/^{144}Nd$, ε_{Nd}, and Mean Grain Size Data in Core MD77-186

Depth (cm)	Age (kyr)	$^{87}Sr/^{86}Sr$	±2σ	$^{143}Nd/^{144}Nd$	±2σ	ε_{Nd}	±2σ	Mean grain size (um)
7–8	5.2	0.7160	1.00E-05	0.512125	1.16E-05	−10.0	0.2	15.0
57–58	6.4	0.7146	1.21E-05	0.512105	1.28E-05	−10.4	0.2	25.2
109–110	8.2	0.7190	1.42E-05	0.512097	1.02E-05	−10.5	0.2	26.6
139–140	10.9	0.7181	1.28E-05	0.512087	1.05E-05	−10.8	0.2	17.1
183–184	14.1	0.7186	1.24E-05	0.512099	1.17E-05	−10.5	0.2	19.0
211–212	15.6	0.7188	1.05E-05	0.512096	1.32E-05	−10.6	0.2	14.2
235–236	17.1	0.7246	1.02E-05	0.512072	1.12E-05	−11.0	0.2	24.4
259–260	19.6	0.7237	1.24E-05	0.512055	1.07E-05	−11.4	0.2	17.5
283–284	21.8	0.7236	1.15E-05	0.512075	8.77E-06	−11.0	0.2	15.7
303–304	23.3	0.7234	1.13E-05	0.512080	9.12E-06	−10.9	0.2	23.3
335–336	26.5	0.7220	1.34E-05	0.512091	9.87E-06	−10.7	0.2	15.2

Note. ε_{Nd} was determined using the present CHUR value from Jacobsen and Wasserburg (1980): $\varepsilon_{Nd}(0) = [(^{143}Nd/^{144}Nd)_{meas}/0.512638 - 1] * 10{,}000$.

signatures from 0.706 to 0.718 and radiogenic ε_{Nd} from −8 to −1 (Allen et al., 2008; Licht et al., 2013). The Irrawaddy River sediments display $^{87}Sr/^{86}Sr$ and ε_{Nd} from 0.712 to 0.721 and −12 to −9, respectively (Colin et al., 1999; Damodararao et al., 2016), very similar to that of detrital fractions at site MD77-186 (Figure 4c). Previous studies of deep-sea cores have suggested that the sediment discharge of the Irrawaddy River could be possibly transported to the eastern BoB by the clockwise ocean circulation induced by the summer monsoon (Ahmad et al., 2005; Colin et al., 1999). Therefore, sediments from the Irrawaddy River could also contribute to the detrital sedimentation at site MD77-186. However, we argue that the Irrawaddy River is unlikely to represent a dominant source of sediment at core MD77-186, due to the barrier effect of the shallow water strait on the presumed flow trajectory of Irrawaddy River sediments from the Andaman Sea to the BoB.

Sediment inputs from the Indian Peninsula rivers, such as the Krishna and Godavari rivers, are presumably negligible for core MD77-186, considering their reduced sediment loads and the long distance to the eastern BoB. The sediment discharge of the Indian Peninsula rivers (total sediment discharge of 2.4×10^8 t/year) is generally one order of magnitude smaller than the G-B River (sediment discharge of 1.1×10^9 t/year) (Tripathy et al., 2011). Moreover, Sr-Nd isotopes studies of core MD77-176 located in the northeast BoB (Colin et al., 2006) and core SK-157-14, located in the southeast BoB (Ahmad et al., 2005), also indicate a negligible contribution of sediment from Indian Peninsula rivers during the LGM and Holocene. The Andaman Islands consist of an extensive succession of faulted and sheared turbiditic sand stones and mudrocks (Garzanti et al., 2013), with associated $^{87}Sr/^{86}Sr$ and ε_{Nd} sediment signatures around ~0.705 and ~−5 (Ali et al., 2015; Allen et al., 2008). However, there are no large rivers in the Andaman Islands that could act as a significant sediment contributor to the BoB (Ahmad et al., 2005; Sebastian et al., 2019). Moreover, a recent investigation of Sr, Nd, and Pb isotopes in the detrital clay-size fraction and clay mineral assemblages have shown that the Andaman Islands only contributed negligible amounts of clays to the nearby ocean margins during the late Quaternary (Ali et al., 2015). Therefore, we can reasonably exclude the Andaman Islands as an important sediment source for cores MD77-186 and MD77-171.

In addition, the detrital sedimentation at the MD77-171 site in the Andaman Sea mainly falls under the influence of the sediment supplies derived by the Indo-Burman Ranges and the Irrawaddy River (Colin et al., 1999; Damodararao et al., 2016). Such a conclusion is also supported by previous investigations of nearby sediment cores, for example, SK234/60 (Awasthi et al., 2014), NGHP01-17A (Ali et al., 2015; Sebastian et al., 2019), and MD77-169 (Colin et al., 1999, 2006).

A key observation in Figure 4c is that $^{87}Sr/^{86}Sr$ ratios of MD77-186 (red circles) are higher during the LGM (0.7235 ± 0.0010, $n = 5$) than during the subsequent warmer time interval (0.7175 ± 0.0020, $n = 6$). This finding is also evident in nearby cores MD77-176 (blue rhombuses in Figure 4c) and SK157-14 (green triangles in Figure 4c), indicating that the same feature is ubiquitous in the eastern BoB. A deeper penetration of monsoon precipitation into the Himalayan ranges during the post-LGM period would have possibly resulted in sediments being characterized by higher $^{87}Sr/^{86}Sr$ values, as opposed to our observation. Considering that

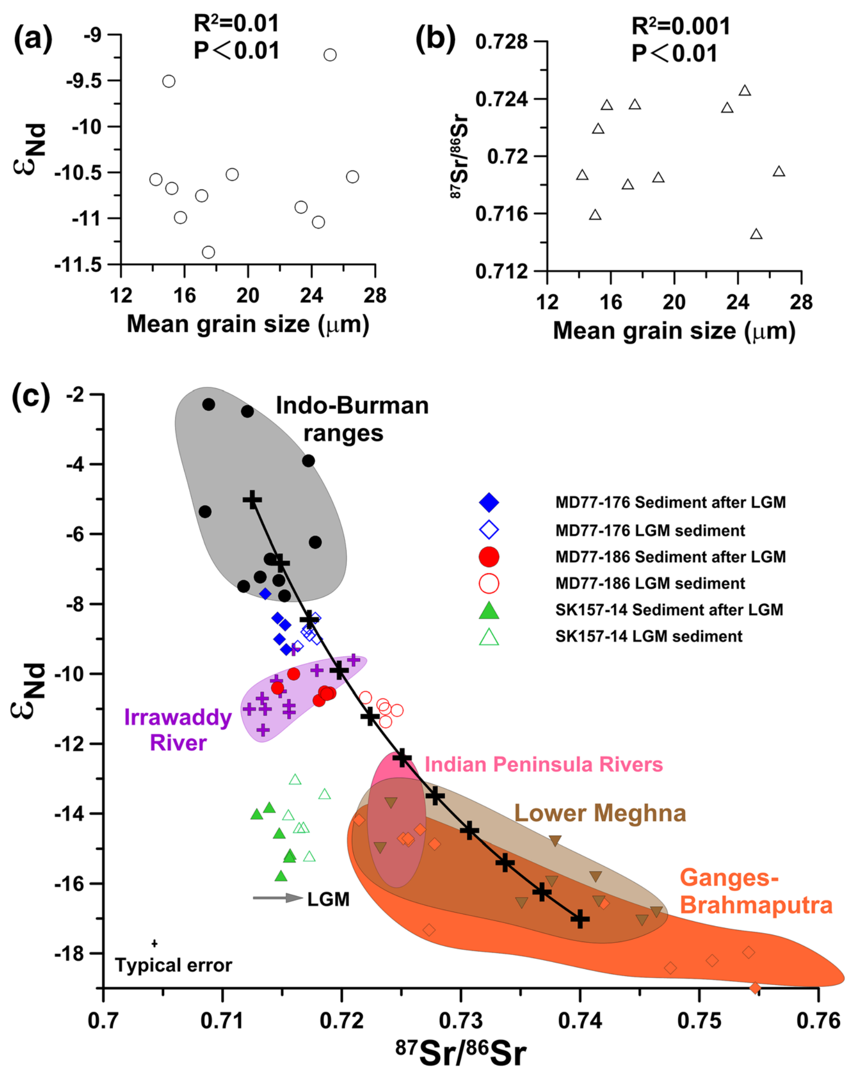

Figure 4. (a) ε_{Nd} and (b) $^{87}Sr/^{86}Sr$ versus mean grain size in core MD77-186. Sr-Nd isotopes show no significant correlations with mean grain size, suggesting a negligible influence of grain size sorting on the isotopic compositions in core MD77-186. (c) $^{87}Sr/^{86}Sr$ versus ε_{Nd} in detrital sediments from core MD77-186 (this study), together with reference data from previously published studies: cores MD77-176 (Colin et al., 2006) and SK157-14 (Ahmad et al., 2005), Indian Peninsula rivers (Ahmad et al., 2009), Ganges-Brahmaputra River and Lower Meghna (Lupker et al., 2013), and Irrawaddy River (Colin et al., 1999; Damodararao et al., 2016). Note that the results obtained during both Last Glacial Maximum (LGM) and post-LGM intervals in cores MD77-176, MD77-186, and SK157-14 display near-constant ε_{Nd} compositions but different $^{87}Sr/^{86}Sr$ ratios, respectively.

the ε_{Nd} in these cores have remained nearly constant since the LGM (−8.7 ± 0.4 for core MD77-176 (Colin et al., 2006); −10.7 ± 0.4 for MD77-186 [this study]; −14.4 ± 0.8 for SK157-14 (Ahmad et al., 2005)), one can reasonably exclude that the observed downcore $^{87}Sr/^{86}Sr$ shifts reflect any major change in sediment sources and/or the impact of different ocean circulation patterns on detrital sedimentation. Furthermore, a reworking of deltaic or continental shelf sediments during sea level lowstands could have also affected the sedimentation in the eastern BoB as previously suggested for the Arabian Sea (Alizai et al., 2012) and the South China Sea (Wan et al., 2017). However, such mechanism seems to be insignificant in the BoB as its continental shelves are very narrow (average less than 20 km) and because most of the sediment load is transported through a major canyon system called the "Swatch of No Ground." Consequently, the observed detrital $^{87}Sr/^{86}Sr$ change in the eastern BoB since the LGM is probably best explained by changes in the degree of chemical weathering in Himalayan river basins.

10.1029/2020GC008936

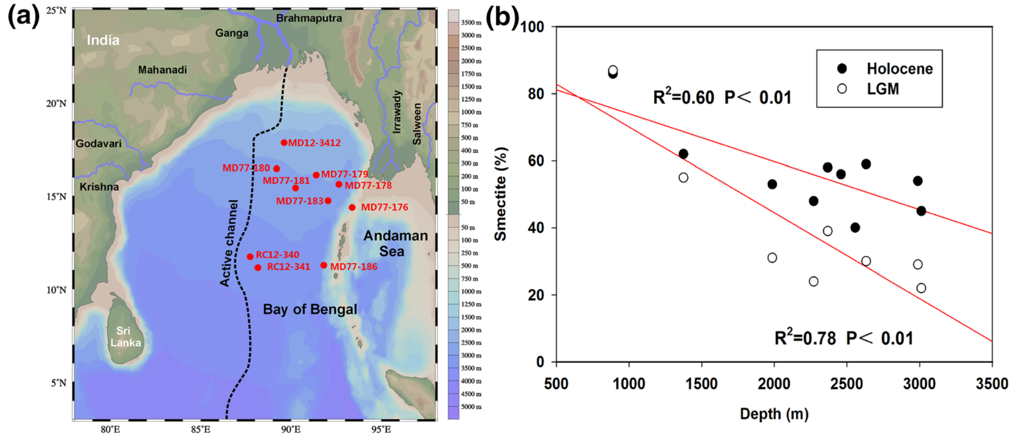

Figure 5. (a) Cores that are used to compare smectite (%) in the eastern BoB and (b) smectite (%) versus water depth (m) in the eastern BoB. Note that they are located on two different fitting lines during Holocene and LGM, respectively.

During the LGM and other past glacial periods, reduced monsoonal rainfall and temperature most likely led to slower chemical weathering in South Asian river basins, while enhanced physical erosion prevailed in the Himalayas in response to glacial scour and frost action (Colin et al., 2006; Lupker et al., 2013; Prestrud Anderson et al., 1997). At that time, the combination of reduced rock weathering and greater physical erosion in the highlands of Himalaya would have resulted in increasing export of less-altered radiogenic Rb-rich minerals (i.e., characterized by relatively high $^{87}Sr/^{86}Sr$ ratios) such as biotite, thereby explaining the observed shift toward higher $^{87}Sr/^{86}Sr$ ratios compared to Holocene sediments (Colin et al., 2006; Prestrud Anderson et al., 1997). We argue that enhanced physical erosion during the LGM could have enhanced the exposure of fresh rock surface, resulting in reduced weathering intensities. This is supported by studies of sediment cores from the upper Bengal deep-sea fan, which have previously shown that sediments derived from Himalaya river system during the LGM were less weathered than Holocene sediments (Joussain et al., 2016; Lupker et al., 2013).

4.2. Significance of the Variations in Clay Mineralogy

The scenario linking detrital $^{87}Sr/^{86}Sr$ ratios to changing weathering patterns in South Asia is supported by observed variations in clay mineral assemblages at sites MD77-186 and MD77-171. In large South Asian rivers, detrital illite and chlorite are mainly produced by the alteration of crystalline source rocks and/or recycled from ancient sedimentary rocks through physical erosion processes in the Himalayan highlands (Colin et al., 1999; Huyghe et al., 2011). In contrast, smectite neoformation mostly occurs in the thicker soil sequences located downstream in the floodplains, where more humid conditions result in intense chemical weathering (Colin et al., 1999; Huyghe et al., 2011). The middle and lower reaches of the Ganges River are enriched in smectite as indicated by Sarin et al. (1989) and Huyghe et al. (2011), which mainly comes from recycling of smectite-rich sedimentary deposits and pedogenesis in the Ganges River plain. Such formation of smectite results from a higher residence time of sediments in the floodplain, hence leaving sufficient time for silicate weathering and clay mineral formation to proceed (Huyghe et al., 2011). Consequently, the smectite/(illite + chlorite) ratio can be used as a weathering proxy indicative of the relative contribution of detrital material derived from high mountains versus floodplains in Himalayan river systems.

Measured smectite abundances in cores MD77-186 and MD77-171 indicate high contents (generally more than 60%) potentially accounted for by sediment delivery from the Indo-Burman Ranges. Unfortunately, to the best of our knowledge, there is no data on clay mineral assemblages associated with the Indo-Burman Ranges, so that we cannot verify this hypothesis. Another possible explanation for the high smectite content could be a particle sorting effect during its transportation by currents. For a constant sediment source, under strong current velocities, sediments could contain a higher proportion of smectite to their small particle size as revealed by studies in the Amazon River (Gibbs, 1977) and in the South China Sea (Schroeder et al., 2015). Moreover, we have plotted smectite contents versus the water depth of corresponding sediment cores (n = 10) for the eastern BoB during both the LGM and Holocene (Figure 5). We

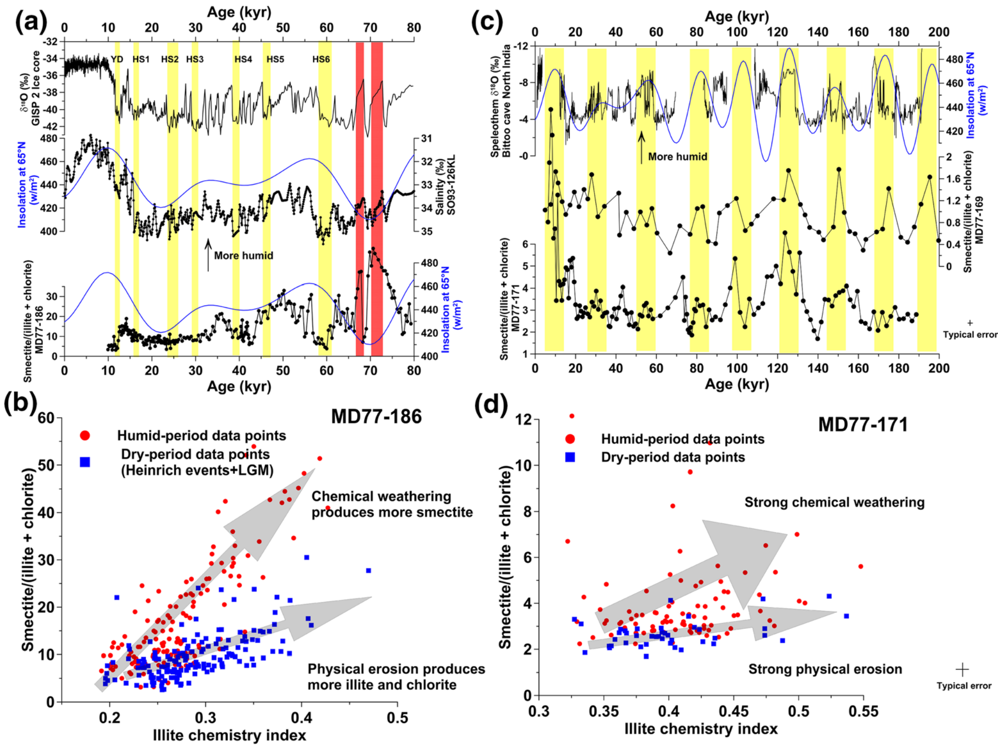

Figure 6. (a) Comparison of smectite/(illite + chlorite) ratios from core MD77-186 (this study) with sea surface salinity proxy reconstructed from core SO93-126KL (Kudrass et al., 2001), Greenland ice core δ^{18}O record GISP2 (Grootes & Stuiver, 1997), and insolation at 65°N in July (Laskar et al., 2004). The HS1-6 and YD cold events in the Northern Hemisphere are marked by yellow bars, while two warm and humid events but corresponding to lower insolation from 75 to 65 kyr are marked by red bars. (b) Smectite/(illite + chlorite) ratios versus illite chemistry index in core MD77-186. Dry-blue dots are data points in Heinrich events and LGM, while humid-red dots are the other data points. (c) Comparison of smectite/(illite + chlorite) ratios from core MD77-171 (this study) and nearby core MD77-169 (Colin et al., 1999), Indian summer rainfall record reconstructed from Bittoo cave stalagmite since 190 kyr (Kathayat et al., 2016), and insolation at 65°N in July (Laskar et al., 2004). Note that the peaks of those records generally correspond to insolation maxima. (d) Smectite/(illite + chlorite) ratios versus illite chemistry index in core MD77-171. Dry-blue dots are data points in low Bittoo cave stalagmite reconstructed rainfall, while humid-red dots are the other data points. Note that the dry- and humid-period data points in (b) and (d) are defined by the comparison of rainfall proxy and smectite/(illite + chlorite) ratios in (a) and (c), respectively. Both (b) and (d) exhibit two distinct scatter plots, indicating that they are induced by different mechanisms.

found that the smectite contents show a good correlation with core water depth ($R^2 = 0.60$, $p < 0.01$ for the Holocene and $R^2 = 0.78$, $p < 0.01$ for the LGM, Figure 5), supporting the particle sorting hypothesis of smectite by ocean currents. A mechanism of preferential capture of smectite close to the river mouth, recently found in the Indus River canyon and delta (Li et al., 2019), is probably not applicable in our study as these eastern BoB cores are located far from the river mouth. Furthermore, the smectite contents during the Holocene are slightly higher than their LGM ones, consistent with the increase of smectite in floodplain during humid and warm Holocene although sediments in the floodplains are also originally derived from highlands of Himalaya.

To further explore the potential linkage between mountain- versus floodplain-dominated weathering regimes and climate, we compare measured smectite/(illite + chlorite) ratios to rainfall proxies for the ISM and the 65°N summer insolation signal (Figure 6). Estimates for sea surface salinity (SSS) in a nearby core from the northern BoB (Figure 1) (Kudrass et al., 2001), which recorded past fluctuations in monsoonal freshwater discharge from the G-B River, shows strong correlation with the evolution of Northern Hemisphere temperature inferred from both GISP2 δ^{18}O record (Grootes & Stuiver, 1997) and 65°N insolation (Laskar et al., 2004) (Figure 6a). The trend for smectite/(illite + chlorite) ratios in core MD77-186 matches well with both the SSS record and 65°N summer insolation, with higher smectite/(illite + chlorite) ratios generally corresponding to SSS minima (and inferred enhanced monsoonal precipitation and freshwater discharge), and vice versa (Figure 6a). In contrast, past short-term cold events,

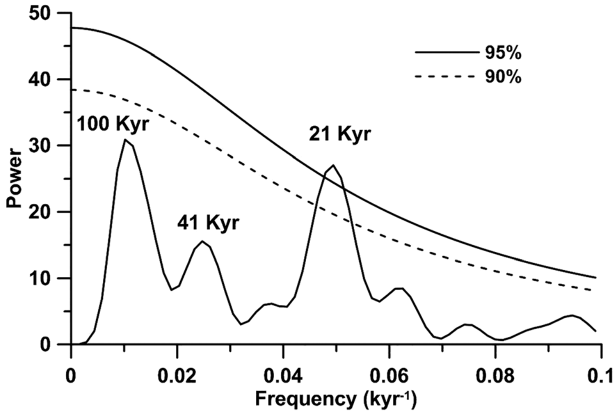

Figure 7. Spectral analysis of smectite/(illite + chlorite) ratios in core MD77-171. Note the dominant 21- and 100-kyr cycles.

such as Heinrich Stadials (HS1-6) and the Younger Dryas (YD), are associated with higher SSS (i.e., reduced monsoonal precipitation) and lower smectite/(illite + chlorite) ratios in core MD77-186.

On the other hand, we also observe two pronounced millennial-scale excursions from 75 to 65 kyr, during which smectite/(illite + chlorite) ratios in core MD77-186 increase concomitantly with lower SSS and higher GISP2 δ^{18}O (i.e., indicative of enhanced precipitation and warmer northern hemisphere high latitudes), but in a period characterized by low insolation at 65°N (see the red bars in Figure 6a). Similarly conflicting observations between both the smectite/(illite + chlorite) ratios and the summer insolation from 75 to 65 kyr were also apparent in cores MD77-169 and MD77-171 (Figure 6c), implying that they correspond most likely to a regional feature. This observation suggests that coincident co-variations of Northern Hemisphere temperatures and ISM intensity from 75 to 65 kyr were probably not responding to 65°N insolation forcing. Nevertheless, the roughly synchronous variations observed for smectite/(illite + chlorite) ratios in core MD77-186 and regional SSS proxy data clearly show that weathering patterns in large Himalayan river basins can respond rapidly to short-term climate changes. Previous investigations of river systems from temperate regions have documented long time lags (10^5–10^6 years) and sign attenuation due to the buffering and recycling of sediments within catchments during source-to-sink transport processes (Bi et al., 2015; Castelltort & Van Den Driessche, 2003; Dosseto et al., 2006, 2010; Granet et al., 2010; Li et al., 2016), implying that shorter-term climate changes could not be reflected in the marine sediment records. However, in the monsoon-influenced South Asia river systems, sediments (in particularly the finest clay-size particles) are generally efficiently transported to the ocean with limited storage within the basin, suggesting that proximal sediment sequences deposited in nearby ocean margins may represent suitable archives for investigating short-term climate changes (Goodbred, 2003). Such conclusion is also supported by other marine sedimentary records from the Arabian sea (Caley et al., 2011; Prins et al., 2000) and BoB (Joussain et al., 2016; Lupker et al., 2013).

Similarly, over the last 190 kyr, smectite/(illite + chlorite) ratios in core MD77-171 (Figure 1) also follow closely both the 65°N summer insolation and the ISM rainfall record reconstructed from Bittoo cave speleothems in Northern India (Figure 6c) (Kathayat et al., 2016). In agreement with results obtained on a nearby core (MD77-169) in the Andaman Sea (Colin et al., 1999), spectral analysis of smectite/(illite + chlorite) ratios in MD77-171 demonstrates dominant 21- and 100-kyr cycles (Figure 7), which suggest that the ISM acted as a major forcing mechanism on weathering and erosion patterns in large Himalayan river basins during the late Quaternary.

Additional information can be gained from the illite chemistry index (Figures 6b and 6d). These values are systematically smaller than 0.5, hence indicative of Fe-Al-rich illite produced by physical erosion of low-grade metamorphic rocks in the highlands of Himalaya (Colin et al., 1999; Huyghe et al., 2011). While the downcore evolution of the illite chemistry index closely follows smectite/(illite + chlorite) ratios (Figure 3), the two parameters display two separate trends when plotted versus each other (Figures 6b and 6d), corresponding to dry (data points in Heinrich events and LGM for core MD77-186, while data points in low Bittoo cave stalagmite reconstructed rainfall) and humid periods (other data points), respectively. For any given value of illite chemistry index, humid periods are generally associated with higher smectite/(illite + chlorite) ratios compared to corresponding values for dry episodes. This interesting observation adds further support to our hypothesis that the intensification of chemical weathering during periods of enhanced ISM mostly took place in the floodplains, while the relative contribution of detrital sediment derived from upstream high mountain environments increased during the dryer glacial periods, probably due to stronger physical erosion in Himalaya highlands.

4.3. Climate-Driven Weathering Shifts Between Highlands and Floodplains

To summarize the lines of evidence outlined above, (i) the observed ^{87}Sr/^{86}Sr shift from LGM to Holocene toward less radiogenic compositions (Figure 4c), (ii) the synchronous variations of smectite/(illite + chlorite) ratios with SSS (Figure 6a) and monsoon precipitation (Figure 6c) in the

10.1029/2020GC008936

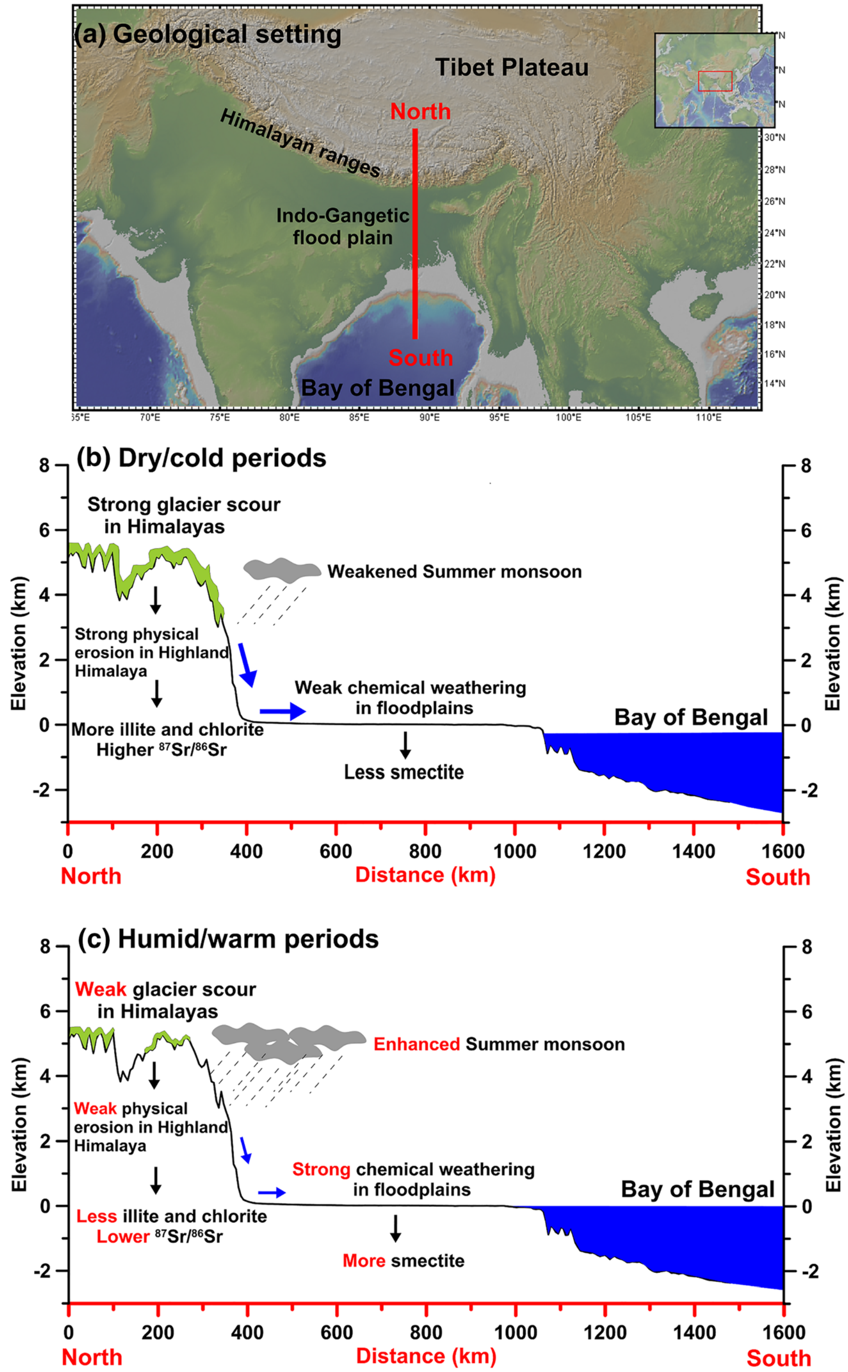

Figure 8. Schematic diagram showing the alternation between high mountain- versus floodplain-dominated weathering regimes in large Himalayan river basins. (a) Simplified geological setting. Note that the red line corresponds to the transect chosen as an example; (b) high mountain-dominated erosional pattern during dry/cold periods; and (c) floodplain-dominated weathering pattern during humid/warm periods.

Northern Indian Ocean, and (iii) the two distinct trends for smectite/(illite + chlorite) versus illite chemistry index observed in both humid and dry periods (Figure 6b and 6d) collectively suggest that past climate changes in South Asia were associated with abrupt shifts between high mountain- versus floodplain-dominated weathering regimes. Below, we use a simplistic schematic transect from the Tibetan Plateau, to the floodplain and the BoB to illustrate this mechanism (Figure 8a).

During cold and dry intervals such as Heinrich events and glacial periods (Figure 8b), the combination of lower temperature (Grootes & Stuiver, 1997) and lower monsoonal rainfall (Kudrass et al., 2001) led to slower chemical weathering and smectite formation rates in the floodplains, while glacial erosion accelerated in the Himalayan highlands and favored the export of illite, chlorite (Colin et al., 1999; Huyghe et al., 2011), and less-altered biotite with high $^{87}Sr/^{86}Sr$ ratio (Prestrud Anderson et al., 1997). Instead, during warm and humid periods (Figure 8c), shrinking glaciers in Himalayan highlands and enhanced rainfall in the floodplains both led to reduced export of mountain-derived primary minerals (Gabet et al., 2008) and higher production rates of smectite, although the materials deposited in the floodplains could also originally derive from High Himalaya (Colin et al., 1999; Huyghe et al., 2011). The less-weathered sediments exported from the Himalayan highlands during cold periods, which were partly stored in the floodplains, were likely to be efficiently weathered during subsequent warmer time intervals (Lupker et al., 2012; Vance et al., 2009). Combined $^{87}Sr/^{86}Sr$ and ε_{Nd} investigations of the Ganga (Singh et al., 2008) and Brahmaputra river systems (Singh & France-Lanord, 2002) indicate that most of the modern river sediments are derived from the high-topography regions of the Higher Himalayan Crystallines, resulting from monsoon induced high physical erosion rates. Such a mechanism linking the weathering regime to summer monsoon rainfall may only work during the warm interglacial periods. Instead, during cold glacials, our data suggest that glacial scour probably played a more important role in controlling poorly chemical weathered sediments inputs, at times when summer monsoon precipitation was weaker.

Colin et al. (1999) have already proposed a similar climate-driven mechanism for the production of pedogenic clays in the floodplain (smectite and kaolinite) relative to detrital minerals (chlorite, kaolinite, and quartz) in the South Asia area, using both Nd and Sr isotopic and clay mineral data. Additionally, in this study, our data also suggest that both weathering and erosion processes in large river basins can also respond rapidly to short-term climate forcing, a finding that echoes with results obtained recently in other investigations conducted in the Himalaya (Dosseto et al., 2015), the Congo River (Bayon et al., 2012), and the Nile River (Bastian et al., 2017) basins, using silicate weathering proxies. In a novel departure, we propose here that the climate-driven erosional shifts identified in South Asian river basins during the late Quaternary were also accompanied by the alternation between high mountain- versus floodplain-dominated weathering regimes. A similar mechanism is likely to also have operated in other large river basins in the past, such as in the Amazon River (Bouchez et al., 2012; Gaillardet et al., 1997; Torres et al., 2016), the Nile River (Bastian et al., 2017), and the Congo River (Bayon et al., 2012) basins, despite marked differences in corresponding elevation, hydrologic cycle, and main lithological composition.

The alteration of silicate rocks on continents is generally considered to play a role in controlling atmospheric CO_2 concentrations over geologic timescales (Garrels et al., 1976; Raymo & Ruddiman, 1992; West et al., 2005). Presumably, the alternation between high mountain- versus floodplain-dominated weathering regimes over glacial–interglacial timescales could also have had an important impact on atmospheric CO_2, because glacial erosion in mountains can act as a net source of CO_2 to the atmosphere, through oxidation of sulfide minerals (Torres et al., 2014, 2017) and petrogenic organic carbon hosted by sedimentary rocks (Bouchez et al., 2010; Horan et al., 2017), while floodplains can be viewed as silicate weathering reactors and atmospheric CO_2 sinks (Bouchez et al., 2012). Recently, a study of rhenium in the mountainous watersheds of New Zealand to track the oxidation of rock-bound organic carbon has shown that glacial activity in high mountain environments could act as a net source of atmospheric CO_2 source through weathering of sedimentary rocks (Horan et al., 2017). The Himalayas host both mountain glaciers and abundant organic-rich sedimentary rock sequences in high-topography regions (Beck et al., 1995; Joussain et al., 2016). On this basis, we speculate that enhanced physical erosion in Himalaya highlands and other high mountain environments worldwide during past glacial periods were possibly accompanied by substantial CO_2 inputs to the atmosphere, while the onset of warmer and more humid conditions in the past coincided with a shift toward floodplain-dominated silicate weathering, which could have acted instead as a sink for atmospheric CO_2 (Torres et al., 2014, 2016). Future investigations should aim at providing quantitative constraints on the potential impact of climate-driven weathering shifts over glacial–interglacial timescales on global carbon cycling and assess its possible relevance in the context of on-going global warming and shrinking glaciers.

5. Conclusions

Clay mineralogy and strontium-neodymium isotopic compositions of sediments were analyzed from cores MD77-186 and MD77-171 in the Northern Indian Ocean to investigate the weathering response of large Himalayan river basins to orbital and millennial climate forcing. We observe that past glacial periods of the late Quaternary were associated with the export of weakly weathered sediment material from the Himalayan highlands characterized by illite and chlorite-dominated assemblages relatively radiogenic Sr isotopic signatures. In contrast, warm periods of enhanced monsoon rainfall were accompanied by the transport of intensively weathered smectite-rich soils with lower $^{87}Sr/^{86}Sr$ compositions, mostly derived from the floodplains. The alternation between high mountain- versus floodplain-dominated weathering regimes presumably had an impact on the carbon cycle. During glacial periods, enhanced physical erosion in the Himalaya highlands, and its potential influence on the alteration of organic-rich sedimentary rocks, possibly acted as a net source of CO_2 to the atmosphere through oxidation processes, while enhanced silicate weathering in floodplains during warm and humid periods possibly led to more efficient CO_2 sequestration. The potential impact of climate-driven erosional shifts between high mountain- versus floodplain-dominated in large river basins on the carbon cycle during the late Quaternary, as observed in our study, should be further investigated in future studies.

Data Availability Statement

The original data of this study are available at Zenodo (https://doi.org/10.5281/zenodo.3724991) and are also in supporting materials.

Acknowledgments
This work was supported by the National Natural Science Foundation of China (No. 91958107 and 41806060), Laboratory for Marine Geology, Qingdao Pilot National Laboratory for Marine Science and Technology (No. MGQNLM-TD201902), Open Fund of the State Key Laboratory of Marine Geology, Tongji University (No. MGK1919), Youth Innovation Promotion Association, Chinese Academy of Sciences (No. 2020210), and Open Fund of the Key Laboratory of Marine Geology and Environment, Chinese Academy of Sciences (No. MGE2018KG01). C.C. was supported by the National Research Agency L-IPSL Project (ANR-10-LABX-0018) and MONOPOL Project (ANR 2011 Blanc SIMI 5-6 024 04). We especially thank Louise Bordier and Arnaud Dapoigny for their assistance in Sr and Nd isotopic composition measurements as well as Olivier Dufour and Serge Miska for XRD analyses. We also thank the valuable comments from Editor Adina Paytan, Dr. Anthony Dosseto, and one anonymous reviewer.

References

Ahmad, S. M., Babu, G. A., Padmakumari, V. M., Dayal, A. M., Sukhija, B. S., & Nagabhushanam, P. (2005). Sr, Nd isotopic evidence of terrigenous flux variations in the Bay of Bengal: Implications of monsoons during the last ∼34,000 years. *Geophysical Research Letters*, *32*, L22711. https://doi.org/10.1029/2005gl024519

Ahmad, S. M., Padmakumari, V., & Babu, G. A. (2009). Strontium and neodymium isotopic compositions in sediments from Godavari, Krishna and Pennar rivers. *Current Science*, *97*(12).

Ali, S., Hathorne, E. C., Frank, M., Gebregiorgis, D., Stattegger, K., Stumpf, R., et al. (2015). South Asian monsoon history over the past 60 kyr recorded by radiogenic isotopes and clay mineral assemblages in the Andaman Sea. *Geochemistry, Geophysics, Geosystems*, *16*, 505–521. https://doi.org/10.1002/2014GC005586

Alizai, A., Hillier, S., Clift, P. D., Giosan, L., Hurst, A., VanLaningham, S., & Macklin, M. (2012). Clay mineral variations in Holocene terrestrial sediments from the Indus Basin. *Quaternary Research*, *77*(3), 368–381. https://doi.org/10.1016/j.yqres.2012.01.008

Allen, A., Carter, Y., Najman, P., Bandopadhyay, H., Chapman, M., Bickle, E., et al. (2008). New constraints on the sedimentation and uplift history of the Andaman-Nicobar accretionary prism. *South Andaman Island, Special papers-geological society of America*, *436*, 223. https://doi.org/10.1130/2008.2436(11)

Allen, Y., Najman, A., Carter, D., Barfod, M., Bickle, J., Chapman, H. J., et al. (2008). Provenance of the Tertiary sedimentary rocks of the Indo-Burman Ranges, Burma (Myanmar): Burman arc or Himalayan-derived? *Journal of the Geological Society*, *165*(6), 1045–1057. https://doi.org/10.1144/0016-76492007-143

Awasthi, N., Ray, J. S., Singh, A. K., Band, S. T., & Rai, V. K. (2014). Provenance of the Late Quaternary sediments in the Andaman Sea: Implications for monsoon variability and ocean circulation. *Geochemistry, Geophysics, Geosystems*, *15*, 3890–3906. https://doi.org/10.1002/2014gc005462

Bastian, L., Revel, M., Bayon, G., Dufour, A., & Vigier, N. (2017). Abrupt response of chemical weathering to Late Quaternary hydroclimate changes in northeast Africa. *Scientific Reports*, *7*, 44,231. https://doi.org/10.1038/srep44231

Bayon, G., Dennielou, B., Etoubleau, J., Ponzevera, E., Toucanne, S., & Bermell, S. (2012). Intensifying weathering and land use in Iron Age Central Africa. *Science*, *335*(6073), 1219–1222. https://doi.org/10.1126/science.1215400

Beaulieu, E., Goddéris, Y., Donnadieu, Y., Labat, D., & Roelandt, C. (2012). High sensitivity of the continental-weathering carbon dioxide sink to future climate change. *Nature Climate Change*, *2*(5), 346–349. https://doi.org/10.1038/nclimate1419

Beck, R. A., Burbank, D. W., Sercombe, W. J., Olson, T. L., & Khan, A. M. (1995). Organic carbon exhumation and global warming during the early Himalayan collision. *Geology*, *23*(5), 387–390. https://doi.org/10.1130/0091-7613(1995)023%3C0387:oceagw%3E2.3.co;2

Bi, L., Yang, S., Li, C., Guo, Y., Wang, Q., Liu, J. T., & Yin, P. (2015). Geochemistry of river-borne clays entering the East China Sea indicates two contrasting types of weathering and sediment transport processes. *Geochemistry, Geophysics, Geosystems*, *16*, 3034–3052. https://doi.org/10.1002/2015gc005867

Bouchez, J., Beyssac, O., Galy, V., Gaillardet, J., France-Lanord, C., Maurice, L., & Moreira-Turcq, P. (2010). Oxidation of petrogenic organic carbon in the Amazon floodplain as a source of atmospheric CO_2. *Geology*, *38*(3), 255–258. https://doi.org/10.1130/G30608.1

Bouchez, J., Gaillardet, J., Lupker, M., Louvat, P., France-Lanord, C., Maurice, L., et al. (2012). Floodplains of large rivers: Weathering reactors or simple silos? *Chemical Geology*, *332–333*, 166–184. https://doi.org/10.1016/j.chemgeo.2012.09.032

Broecker, W. S., & Peng, T. H. (1982). *The tracers in the sea*. Palisades, NY: Lamont Doherty Geological Observatory.

Burbank, D. W., Blythe, A. E., Putkonen, J., Pratt-Sitaula, B., Gabet, E., Oskin, M., et al. (2003). Decoupling of erosion and precipitation in the Himalayas. *Nature*, *426*(6967), 652–655. https://doi.org/10.1038/nature02187

Burton, K. W., & Vance, D. (2000). Glacial–interglacial variations in the neodymium isotope composition of seawater in the Bay of Bengal recorded by planktonic foraminifera. *Earth and Planetary Science Letters*, *176*(3-4), 425–441. https://doi.org/10.1016/S0012-821X(00)00011-X

Caley, T., Malaizé, B., Zaragosi, S., Rossignol, L., Bourget, J., Eynaud, F., et al. (2011). New Arabian Sea records help decipher orbital timing of Indo-Asian monsoon. *Earth and Planetary Science Letters*, *308*(3-4), 433–444. https://doi.org/10.1016/j.epsl.2011.06.019

Castelltort, S., & Van Den Driessche, J. (2003). How plausible are high-frequency sediment supply-driven cycles in the stratigraphic record? *Sedimentary Geology*, *157*(1-2), 3–13. https://doi.org/10.1016/S0037-0738(03)00066-6

Clemens, S., Prell, W., Murray, D., Shimmield, G., & Weedon, G. (1991). Forcing mechanisms of the Indian Ocean monsoon. *Nature*, *353*(6346), 720–725. https://doi.org/10.1038/353720a0

Colin, C., Turpin, L., Bertaux, J., Desprairies, A., & Kissel, C. (1999). Erosional history of the Himalayan and Burman ranges during the last two glacial–interglacial cycles. *Earth and Planetary Science Letters*, *171*(4), 647–660. https://doi.org/10.1016/S0012-821X(99)00184-3

Colin, C., Turpin, L., Blamart, D., Frank, N., Kissel, C., & Duchamp, S. (2006). Evolution of weathering patterns in the Indo-Burman Ranges over the last 280 kyr: Effects of sediment provenance on $^{87}Sr/^{86}Sr$ ratios tracer. *Geochemistry, Geophysics, Geosystems*, *7*, Q03007. https://doi.org/10.1029/2005gc000962

Damodararao, K., Singh, S. K., Rai, V. K., Ramaswamy, V., & Rao, P. S. (2016). Lithology, monsoon and sea-surface current control on provenance, dispersal and deposition of sediments over the Andaman continental shelf. *Frontiers in Marine Science*, *3*(118). https://doi.org/10.3389/fmars.2016.00118

Deplazes, G., Lückge, A., Stuut, J.-B. W., Pätzold, J., Kuhlmann, H., Husson, D., et al. (2014). Weakening and strengthening of the Indian monsoon during Heinrich events and Dansgaard-Oeschger oscillations. *Paleoceanography*, *29*, 99–114. https://doi.org/10.1002/2013pa002509

Dosseto, A., Bourdon, B., Gaillardet, J., Maurice-Bourgoin, L., & Allegre, C. J. (2006). Weathering and transport of sediments in the Bolivian Andes: Time constraints from uranium-series isotopes. *Earth and Planetary Science Letters*, *248*(3–4), 759–771. https://doi.org/10.1016/j.epsl.2006.06.027

Dosseto, A., Hesse, P., Maher, K., Fryirs, K., & Turner, S. (2010). Climatic and vegetation control on sediment dynamics during the last glacial cycle. *Geology*, *38*(5), 395–398. https://doi.org/10.1130/G30708.1

Dosseto, A., Vigier, N., Joannes-Boyau, R., Moffat, I., Singh, T., & Srivastava, P. (2015). Rapid response of silicate weathering rates to climate change in the Himalaya. *Geochemical Perspectives Letters*, *1*(0), 10–19. https://doi.org/10.7185/geochemlet.1502

Gabet, E. J., Burbank, D. W., Pratt-Sitaula, B., Putkonen, J., & Bookhagen, B. (2008). Modern erosion rates in the High Himalayas of Nepal. *Earth and Planetary Science Letters*, *267*(3), 482–494. https://doi.org/10.1016/j.epsl.2007.11.059

Gaillardet, J., Dupre, B., Allegre, C. J., & Négrel, P. (1997). Chemical and physical denudation in the Amazon River Basin. *Chemical Geology*, *142*(3), 141–173. https://doi.org/10.1016/S0009-2541(97)00074-0

Gaillardet, J., Dupré, B., Louvat, P., & Allègre, C. J. (1999). Global silicate weathering and CO_2 consumption rates deduced from the chemistry of large rivers. *Chemical Geology*, *159*(1), 3–30. https://doi.org/10.1016/S0009-2541(99)00031-5

Garrels, R. M., Lerman, A., & Mackenzie, F. T. (1976). Controls of atmospheric O_2 and CO_2: Past, present, and future. *American Scientist*, *64*, 306–315.

Garzanti, E., Limonta, M., Resentini, A., Bandopadhyay, P. C., Najman, Y., Andò, S., & Vezzoli, G. (2013). Sediment recycling at convergent plate margins (Indo-Burman Ranges and Andaman–Nicobar Ridge). *Earth-Science Reviews*, *123*, 113–132. https://doi.org/10.1016/j.earscirev.2013.04.008

Gibbs, R. J. (1977). Clay mineral segregation in the marine environment. *Journal of Sedimentary Research*, *47*(1), 237–243. https://doi.org/10.1306/212f713a-2b24-11d7-8648000102c1865d

Goldstein, S. L., & Hemming, S. R. (2003). Long-lived isotopic tracers in oceanography, paleoceanography, and ice-sheet dynamics. *Treatise on geochemistry*, *6*, 625. https://doi.org/10.1016/b0-08-043751-6/06179-x

Goodbred, S. L. Jr. (2003). Response of the Ganges dispersal system to climate change: A source-to-sink view since the last interstade. *Sedimentary Geology*, *162*(1–2), 83–104. https://doi.org/10.1016/S0037-0738(03)00217-3

Goodbred, S. L. Jr., & Kuehl, S. A. (2000). Enormous Ganges-Brahmaputra sediment discharge during strengthened early Holocene monsoon. *Geology*, *28*(12), 1083–1086. https://doi.org/10.1130/0091-7613(2000)28%3C1083:EGSDDS%3E2.0.CO;2

Granet, M., Chabaux, F., Stille, P., Dosseto, A., France-Lanord, C., & Blaes, E. (2010). U-series disequilibria in suspended river sediments and implication for sediment transfer time in alluvial plains: The case of the Himalayan rivers. *Geochimica et Cosmochimica Acta*, *74*(10), 2851–2865. https://doi.org/10.1016/j.gca.2010.02.016

Grootes, P. M., & Stuiver, M. (1997). Oxygen 18/16 variability in Greenland snow and ice with 10^{-3}- to 10^{5}-year time resolution. *Journal of Geophysical Research*, *102*(C12), 26,455–26,470. https://doi.org/10.1029/97JC00880

Horan, K., Hilton, R. G., Selby, D., Ottley, C. J., Gröcke, D. R., Hicks, M., & Burton, K. W. (2017). Mountain glaciation drives rapid oxidation of rock-bound organic carbon. *Science Advances*, *3*(10), e1701107. https://doi.org/10.1126/sciadv.1701107

Hu, D., Clift, P. D., Böning, P., Hannigan, R., Hillier, S., Blusztajn, J., et al. (2013). Holocene evolution in weathering and erosion patterns in the Pearl River delta. *Geochemistry, Geophysics, Geosystems*, *14*, 2349–2368. https://doi.org/10.1002/ggge.20166

Huyghe, P., Guilbaud, R., Bernet, M., Galy, A., & Gajurel, A. P. (2011). Significance of the clay mineral distribution in fluvial sediments of the Neogene to Recent Himalayan Foreland Basin (west-central Nepal). *Basin Research*, *23*(3), 332–345. https://doi.org/10.1111/j.1365-2117.2010.00485.x

Jacobsen, S. B., & Wasserburg, G. (1980). Sm-Nd isotopic evolution of chondrites. *Earth and Planetary Science Letters*, *50*(1), 139–155. https://doi.org/10.1016/0012-821X(80)90125-9

Joussain, R., Colin, C., Liu, Z. F., Meynadier, L., Fournier, L., Fauquembergue, K., et al. (2016). Climatic control of sediment transport from the Himalayas to the proximal NE Bengal Fan during the last glacial-interglacial cycle. *Quaternary Science Reviews*, *148*, 1–16. https://doi.org/10.1016/j.quascirev.2016.06.016

Kathayat, G., Cheng, H., Sinha, A., Spötl, C., Edwards, R. L., Zhang, H., et al. (2016). Indian monsoon variability on millennial-orbital timescales. *Scientific Reports*, *6*, 24374. https://doi.org/10.1038/srep24374

Kudrass, H. R., Hofmann, A., Doose, H., Emeis, K., & Erlenkeuser, H. (2001). Modulation and amplification of climatic changes in the Northern Hemisphere by the Indian summer monsoon during the past 80 ky. *Geology*, *29*(1), 63–66. https://doi.org/10.1130/0091-7613(2001)029%3C0063:MAAOCC%3E2.0.CO;2

Laskar, J., Robutel, P., Joutel, F., Gastineau, M., Correia, A., & Levrard, B. (2004). A long-term numerical solution for the insolation quantities of the Earth. *Astronomy & Astrophysics*, *428*(1), 261–285. https://doi.org/10.1051/0004-6361:20041335

Li, C., Yang, S., Zhao, J.-x., Dosseto, A., Bi, L., & Clark, T. R. (2016). The time scale of river sediment source-to-sink processes in East Asia. *Chemical Geology*, *446*, 138–146. https://doi.org/10.1016/j.chemgeo.2016.06.012

Li, Y., Clift, P. D., Murray, R. W., Exnicios, E., Ireland, T., & Böning, P. (2019). Asian summer monsoon influence on chemical weathering and sediment provenance determined by clay mineral analysis from the Indus Submarine Canyon. *Quaternary Research*, *1-17*. https://doi.org/10.1017/qua.2019.44

Licht, A., France-Lanord, C., Reisberg, L., Fontaine, C., Soe, A. N., & Jaeger, J.-J. (2013). A palaeo Tibet–Myanmar connection? Reconstructing the Late Eocene drainage system of central Myanmar using a multi-proxy approach. *Journal of the Geological Society*, *170*(6), 929–939. https://doi.org/10.1144/jgs2012-126

Lisiecki, L., & Raymo, M. (2005). A Pliocene-Pleistocene stack of 57 globally distributed benthic $\delta^{18}O$ records. *Paleoceanography*, *20*, PA1003. https://doi.org/10.1029/2004pa001071

Liu, J., He, W., Cao, L., Zhu, Z., Xiang, R., Li, T., et al. (2019). Staged fine-grained sediment supply from the Himalayas to the Bengal Fan in response to climate change over the past 50,000 years. *Quaternary Science Reviews*, *212*, 164–177. https://doi.org/10.1016/j.quascirev.2019.04.008

Lugmair, G., Shimamura, T., Lewis, R., & Anders, E. (1983). Samarium-146 in the early solar system: Evidence from neodymium in the Allende meteorite. *Science*, *222*(4627), 1015–1018. https://doi.org/10.1126/science.222.4627.1015

Lupker, M., France-Lanord, C., Galy, V., Lavé, J., Gaillardet, J., Gajurel, A. P., et al. (2012). Predominant floodplain over mountain weathering of Himalayan sediments (Ganga basin). *Geochimica et Cosmochimica Acta*, *84*, 410–432. https://doi.org/10.1016/j.gca.2012.02.001

Lupker, M., France-Lanord, C., Galy, V., Lavé, J., & Kudrass, H. (2013). Increasing chemical weathering in the Himalayan system since the Last Glacial Maximum. *Earth and Planetary Science Letters*, *365*, 243–252. https://doi.org/10.1016/j.epsl.2013.01.038

Millot, R., Gaillardet, J., Dupré, B., & Allègre, C. J. (2002). The global control of silicate weathering rates and the coupling with physical erosion: New insights from rivers of the Canadian Shield. *Earth and Planetary Science Letters*, *196*(1), 83–98. https://doi.org/10.1016/S0012-821X(01)00599-4

Miriyala, P., Sukumaran, N. P., Nath, B. N., Ramamurty, P. B., Sijinkumar, A. V., Vijayagopal, B., et al. (2017). Increased chemical weathering during the deglacial to mid-Holocene summer monsoon intensification. *Scientific Reports*, *7*(1), 44310. https://doi.org/10.1038/srep44310

Petschick, R., Kuhn, G., & Gingele, F. (1996). Clay mineral distribution in surface sediments of the South Atlantic: Sources, transport, and relation to oceanography. *Marine Geology*, *130*(3–4), 203–229. https://doi.org/10.1016/0025-3227(95)00148-4

Prestrud Anderson, S., Drever, J. I., & Humphrey, N. F. (1997). Chemical weathering in glacial environments. *Geology*, *25*(5), 399–402. https://doi.org/10.1130/0091-7613(1997)025%3C0399:cwige%3E2.3.co;2

Prins, M., Postma, G., Cleveringa, J., Cramp, A., & Kenyon, N. (2000). Controls on terrigenous sediment supply to the Arabian Sea during the late Quaternary: The Indus Fan. *Marine Geology*, *169*(3-4), 327–349. https://doi.org/10.1016/S0025-3227(00)00086-4

Raymo, M. E., & Ruddiman, W. F. (1992). Tectonic forcing of late Cenozoic climate. *Nature*, *359*(6391), 117–122. https://doi.org/10.1038/359117a0

Sarin, M., Krishnaswami, S., Dilli, K., Somayajulu, B., & Moore, W. (1989). Major ion chemistry of the Ganga-Brahmaputra river system: Weathering processes and fluxes to the Bay of Bengal. *Geochimica et Cosmochimica Acta*, *53*(5), 997–1009. https://doi.org/10.1016/0016-7037(89)90205-6

Schroeder, A., Wiesner, M. G., & Liu, Z. (2015). Fluxes of clay minerals in the South China Sea. *Earth and Planetary Science Letters*, *430*, 30–42. https://doi.org/10.1016/j.epsl.2015.08.001

Sebastian, T., Nagender Nath, B., Venkateshwarlu, M., Miriyala, P., Prakash, A., Linsy, P., et al. (2019). Impact of the Indian Summer Monsoon variability on the source area weathering in the Indo-Burman ranges during the last 21 kyr—A sediment record from the Andaman Sea. *Palaeogeography, Palaeoclimatology, Palaeoecology*, *516*, 22–34. https://doi.org/10.1016/j.palaeo.2018.11.035

Singh, S. K., & France-Lanord, C. (2002). Tracing the distribution of erosion in the Brahmaputra watershed from isotopic compositions of stream sediments. *Earth and Planetary Science Letters*, *202*(3-4), 645–662. https://doi.org/10.1016/S0012-821X(02)00822-1

Singh, S. K., Rai, S. K., & Krishnaswami, S. (2008). Sr and Nd isotopes in river sediments from the Ganga Basin: Sediment provenance and spatial variability in physical erosion. *Journal of Geophysical Research*, *113*, F03006. https://doi.org/10.1029/2007jf000909

Stoll, H. M., Vance, D., & Arevalos, A. (2007). Records of the Nd isotope composition of seawater from the Bay of Bengal: Implications for the impact of northern hemisphere cooling on ITCZ movement. *Earth and Planetary Science Letters*, *255*(1-2), 213–228. https://doi.org/10.1016/j.epsl.2006.12.016

Storey, M., Roberts, R. G., & Saidin, M. (2012). Astronomically calibrated $^{40}Ar/^{39}Ar$ age for the Toba supereruption and global synchronization of late Quaternary records. *Proceedings of the National Academy of Sciences*, *109*(46), 18684–18688. https://doi.org/10.1073/pnas.1208178109

Stuiver, M. K., Reimer, P. J., & Braziunas, T. F. (1998). High-precision radiocarbon age calibration for terrestrial and marine samples. *Radiocarbon*, *40*(3), 580–589. https://doi.org/10.1017/s0033822200019172

Tierney, J. E., Pausata, F. S. R., & deMenocal, P. (2015). Deglacial Indian monsoon failure and North Atlantic stadials linked by Indian Ocean surface cooling. *Nature Geoscience*, *9*, 46. https://doi.org/10.1038/ngeo2603

Tipper, E. T., Bickle, M. J., Galy, A., West, A. J., Pomiès, C., & Chapman, H. J. (2006). The short term climatic sensitivity of carbonate and silicate weathering fluxes: Insight from seasonal variations in river chemistry. *Geochimica et Cosmochimica Acta*, *70*(11), 2737–2754. https://doi.org/10.1016/j.gca.2006.03.005

Torres, M. A., Moosdorf, N., Hartmann, J., Adkins, J. F., & West, A. J. (2017). Glacial weathering, sulfide oxidation, and global carbon cycle feedbacks. *Proceedings of the National Academy of Sciences*, *114*(33), 8716–8721. https://doi.org/10.1073/pnas.1702953114

Torres, M. A., West, A. J., Clark, K. E., Paris, G., Bouchez, J., Ponton, C., et al. (2016). The acid and alkalinity budgets of weathering in the Andes–Amazon system: Insights into the erosional control of global biogeochemical cycles. *Earth and Planetary Science Letters*, *450*, 381–391. https://doi.org/10.1016/j.epsl.2016.06.012

Torres, M. A., West, A. J., & Li, G. (2014). Sulphide oxidation and carbonate dissolution as a source of CO_2 over geological timescales. *Nature*, *507*, 346. https://doi.org/10.1038/nature13030

Tripathy, G. R., Singh, S. K., Bhushan, R., & Ramaswamy, V. (2011). Sr–Nd isotope composition of the Bay of Bengal sediments: Impact of climate on erosion in the Himalaya. *Geochemical Journal*, *45*(3), 175–186. https://doi.org/10.2343/geochemj.1.0112

Vance, D., Teagle, D. A. H., & Foster, G. L. (2009). Variable Quaternary chemical weathering fluxes and imbalances in marine geochemical budgets. *Nature*, *458*, 493. https://doi.org/10.1038/nature07828

Wan, S., Clift, P. D., Zhao, D., Hovius, N., Munhoven, G., France-Lanord, C., et al. (2017). Enhanced silicate weathering of tropical shelf sediments exposed during glacial lowstands: A sink for atmospheric CO_2. *Geochimica et Cosmochimica Acta*, *200*, 123–144. https://doi.org/10.1016/j.gca.2016.12.010

West, A. J. (2012). Thickness of the chemical weathering zone and implications for erosional and climatic drivers of weathering and for carbon-cycle feedbacks. *Geology*, *40*(9), 811–814. https://doi.org/10.1130/G33041.1

West, A. J., Galy, A., & Bickle, M. (2005). Tectonic and climatic controls on silicate weathering. *Earth and Planetary Science Letters*, *235*(1), 211–228. https://doi.org/10.1016/j.epsl.2005.03.020

Yu, Z., Colin, C., Wan, S., Saraswat, R., Song, L., Xu, Z., et al. (2019). Sea Level-Controlled Sediment Transport to the Eastern Arabian Sea over the Past 600 Kyr: Clay Minerals and SrNd Isotopic Evidence from IODP Site U1457. *Quaternary Science Reviews*, *205*, 22–34. https://doi.org/10.1016/j.quascirev.2018.12.006